Acta Geophysica
https://doi.org/10.1007/s11600-023-01199-x

RESEARCH ARTICLE - SPECIAL ISSUE

Methodology to monitor the seismic response to injected carbon dioxide

Model and synthetic seismograms of CO_2 injection

Mamdoh Alajmi[1] · Davide Gei[3] · José M. Carcione[2,3] · Ayman N. Qadrouh[1] · Juan Santos[2,4,5] · Jing Ba[2]

Received: 31 May 2023 / Accepted: 26 September 2023

Abstract
Petrophysics and fluid-flow simulations are used to build a realistic pre- and post- CO_2 injection geological model for the Utsira formation at the Sleipner field, and the Fourier pseudospectral method is employed to compute synthetic seismograms. The methodology can be used to perform a seismic sensitivity analysis for the detection of carbon dioxide. We built the model solely based on the porosity and clay content of the formations with the aid of fluid-flow and seismic simulations. The pressure map before the injection is assumed to be hydrostatic for which a reference porosity map is defined. The injection induces pore pressure variations and partial saturation, which affect the poroelastic properties and hence the associated seismic response. A proper porosity–permeability–clay content relation is one of the key factors since permeability determines the preferential flow directions and the distribution of the CO_2 plume. The petrophysical model is based on a shaly sandstone (or sandy shale) to represent the caprock, Utsira Sand and embedded mudstone layers. The composite permeability (anisotropic) is analogous to the inverse electrical resistance model. Gas viscosity depends on pressure and temperature. The *P*- and *S*-wave velocities are obtained from Gassmann equation (pre-injection) and White's mesoscopic model (post-injection), which also yields the *P*-wave quality factor in the case of partial (patchy) saturation. To model a realistic situation, we implement a fractal variation of the porosity and clay content, based on the von Kármán correlation function. We then compare the real and synthetic seismograms (pre-injection and post-injection) and show the effect of attenuation on the seismic data. Simulations and real data show a remarkable match.

Keywords Petrophysics · Seismic modeling · Carbon dioxide · Pseudospectral method

Introduction

Carbon dioxide generated by anthropic activities contributes to the greenhouse effect. Capture and storage in aquifers and reservoirs are one of the solutions to avoid this problem. Geophysical methods can be used to monitor the location and migration of the gas in the underground (Chadwick et al. 2005; Ganguli et al. 2019). A suitable geological model is required to perform this task properly, simulating the geometry and petroelastical properties of the different formations, mainly those of the host formation. The most used monitoring methods involve time-lapse seismic surveys. To perform a correct interpretation, fluid-flow simulations (Savioli and Santos 2011; Savioli et al. 2016) and computation of synthetic seismograms (Carcione et al. 2006) are essential. The first method, based on the Black-oil formulation, needs as

Edited by Dr. Abir Jrad (ASSOCIATE EDITOR) / Prof. Gabriela Fernández Viejo (CO-EDITOR-IN-CHIEF).

✉ Jing Ba
jingba@188.com

[1] KACST, PO Box 6086, Riyadh 11442, Saudi Arabia

[2] School of Earth Sciences and Engineering, Hohai University, Nanjing, China

[3] National Institute of Oceanography and Applied Geophysics – OGS, Trieste, Italy

[4] Facultad de Ingeniería, Instituto del Gas y del Petróleo, Universidad de Buenos Aires, Buenos Aires, Argentina

[5] Department of Mathematics, Purdue University, West Lafayette, USA

Published online: 03 November 2023

input the geometry of the layers, the porosity and permeability maps, the fluid viscosities and the rock compressibilities, and how porosity changes with pore pressure. The result of the computation is the pore pressure and CO_2 saturation at every location of the model (Savioli and Santos 2011). Knowledge of these two variables then allows the generation of a new geological model to simulate the time-lapse seismic response. Another more advanced fluid-flow algorithm, recently developed for modeling CO_2 storage, has been presented by Audigane et al. (2007, 2011), which considers structural, dissolution and mineral trapping mechanisms (Carcione et al. 2023).

The methodology proposed here is applied to the Sleipner field at the North Sea (Chadwick et al. 2005; Carcione et al. 2006) but can be used in other contexts as well. In particular, Dupuy et al. (2017) provide well-log data and have characterized the seismic response. Specifically, the injection at Sleipner began in 1996 at an average rate of 1 million tonnes per year. The injection depth is 1012 m b.s.l (Arts et al. 2008) and gas migrates upwards due to buoyancy effects, accumulating below thin shale (mudstone) layers. These layers allow the gas migration to the top because they are not fully sealing. Audigane et al. (2011) show that after three years of injection, the primary trapping process is structural, with solubilization less than 10 % of the injected mass. Hence, the Black-oil formulation can safely be applied to this field. Other equivalent fluid-flow simulations at Sleipner field have been performed by Arts et al. (2004) using the SIMED II simulator and by Chadwick et al. (2006) using the TOUGH2 simulator. The first authors assumed an average permeability of 3.5 D for the Utsira sand and 1 mD for the intra-reservoir mudstone layers. As mentioned above, the initial flow is upwards due to buoyancy, and when it reaches a shale layer the flow is directed toward the side and CO_2 accumulates below these layers, inducing the strong reflections events observed in the seismograms. These authors transformed the saturation model into a 3D acoustic impedance model using Gassmann equations and computed a synthetic seismogram, which resembles the field data, where the pushdown effect caused by the presence of CO_2 can clearly be observed. Chadwick et al. (2006) have been able to characterize the topmost layer of the CO_2 and quantify its rate of growth. The study suggests that transport through the intra-reservoir mudstones is via a limited number of discrete pathways (openings in the mudstone layers) that became established early in plume evolution.

In this work, we generate the pre-injection geological model from the initial porosity (at hydrostatic pore pressure) and clay content or permeability. The petrophysical model assumes a shaly sand, which represents the Utsira Sand, shale thin layers and cap rock, depending on the clay content. The permeability is assumed to be anisotropic and is obtained from first principles as a function of porosity and grain sizes. We model fractal variations of the Utsira Sand porosity and clay content using a von Kármán autocovariance probability function of high fractal dimension (e.g., Carcione and Gei 2009). The model is calibrated to agree with experimental data (well logs and seismic data), with the pre-injection seismic velocities obtained by using Gassmann equations. After the injection, the CO_2 fluid pressure and saturation are used to obtain the properties of the gas at in situ conditions and the petrophysical properties of the Utsira Sand. These are obtained with White's mesoscopic model to model *P*-wave attenuation due to wave-induced fluid flow (e.g., Carcione 2022). An improvement is to use an extension of White model to angles different from normal incidence (Liao et al. 2023).

We simulate two-phase fluid flow using a stress–strain relation based on Biot's theory of poroelasticity for partial saturation combined with the mass conservation equations (Carcione et al. 2014). To uncouple flow and elastic strain, we use a correction to the stiffness of the medium under conditions of uniaxial strain. The pressure and saturation differential equations are then solved with an explicit time stepping scheme and the Fourier pseudospectral method to compute the spatial derivatives. We assume an initial pressure state and at each time step compute the wetting- and non wetting-fluid pressures at a given saturation. Then, we solve Richards's equation for the non wetting-fluid saturation and proceed to the next time step with the updated saturations values. An alternative is to use the STOMP simulator (Subsurface Transport Over Multiple Phases), which simultaneously solves a conservation equation for each mass component (White et al. 1995). The seismic modeling is based on an isotropic-viscoelastic rheology, and the full wavefield is computed with the pseudospectral method (e.g., Carcione 2022; Carcione et al. 2012).

The combined use of fluid-flow and seismic simulations allows us to obtain a porosity-saturation map such that the synthetic seismogram resembles the real data. Porosity, clay contain and permeability obtained on the basis of these two properties are essential to define the pre- and post-injection geological models.

Petrophysical model

The Utsira formation at the injection site has 280 m thickness (top at 820 m and bottom 1100 m b.s.l.). The sea bottom is located at nearly $z_b = 100$ m depth and the caprock is a sealing unit, a silty-mudstone layer 200 m thick

approximately (Arts et al. 2008). Within the reservoir, there are eight mudstone layers ranging from 1 m thickness to 5 m thickness. We build a geological model to approximately fit the real seismogram [e.g., Fig. 14 of Chadwick et al. (2005)]. In the following, we illustrate the steps based on petrophysical theories.

The pressure-temperature conditions are as follows. The temperature profile is approximately $T = 31.7z + 3.4$, where T is the temperature (in degrees Celsius) and z is the depth (in km b.s.l) (Chadwick et al., 2005; Table 1), which gives a $T = 29$ °C at the top and $T = 38$ °C at the bottom of the formation. The hydrostatic pressure is $p_H = \rho_w g z$, with $\rho_w =$ 1040 kg/m^3 the density of brine and g =9.81 m/s^2 the gravity constant. [We obtain 8 MPa and 11 MPa at the top and bottom, respectively (Arts et al. 2008).] The confining pressure is $p_c = \rho_w g z_b + \bar{\rho} g (z - z_b)$, where $\bar{\rho}$ =2100 kg/m^3 is the average sediment density (taken from well logs). (We obtain 16 MPa and 21 MPa at the top and bottom, respectively.)

The density is given by:

$$\rho = (1 - \phi)\rho_s + \phi \rho_f, \tag{1}$$

where $\phi(z)$ is the porosity, ρ_s is the grain density and ρ_f is the fluid density. The grain density is $\rho_s = 2550$ kg/m^3 (both quartz and clay), while in the Utsira sand:

$$\rho_f = (1 - S_w)\rho_g + S_w \rho_w, \tag{2}$$

where S_w is the water saturation and ρ_g is the gas density, which can be obtained from the van der Waals or Peng–Robinson equations as a function of T and p, where p is the pore pressure (e.g., Carcione et al. 2006; Picotti et al. 2012).

We define the porosity of the Utsira Sand at the hydrostatic pressure (pre-injection) $\phi_0 = \phi(p_H)$ fractal (based on the von Kármán function (e.g., Carcione and Gei 2009), with an average value of 37 % and a variation of ± 1%, where function ϕ is defined below. We consider a clay content C = 5 % for the Utsira Sand, with a fractal variation of ± 5 %.

We then use Krief critical-porosity model to obtain the dry-rock bulk modulus,

$$K_m = K_s (1 - \phi)^{A/(1-\phi)}, \tag{3}$$

where ϕ is the pressure-dependent porosity (see below) and K_s is the arithmetic average of the Hashin–Shtrikman (HS) upper and lower bounds (e.g., Carcione et al. 2006), which gives $K_s = 37$ GPa for the Utsira Sand. All the rocks are formed with quartz (bulk and shear modulus of 39 GPa) and clay (bulk and shear moduli of 15 GPa). The quartz and clay proportions to be considered in the HS equations are $(1 - \phi_0)(1 - C)$ and $(1 - \phi_0)C$, respectively. At $z = 0.85$ km, hydrostatic pressure p_H ($\phi = \phi_0 = 37$ %), $C = 0.05$ and $A =$ 4.5, we have $K_m = 1.36$ GPa for the Utsira Sand, while $C =$ 0.85 and $A = 4.5$ give $K_m = 3.26$ GPa (mudstone layers), but in this case $\phi = \phi_0 = 24$ %.

We assume the grain to be a Poisson medium, i.e., $\mu_s = 3K_s/5$, and set the dry-rock shear modulus as:

$$\mu_m = \mu_s (1 - \phi)^{A/(1-\phi)}. \tag{4}$$

Then, $\mu_s = 22$ GPa and $\mu_m = 0.82$ GPa for the Utsira Sand.

Another critical-porosity model is:

$$K_m = K_s \left(1 - \frac{\phi}{\phi_c}\right), \tag{5}$$

(Mavko et al. 2009), where $\phi_c = 0.384$ is the critical porosity to obtain $K_m = 1.36$ GPa for the sand. This ϕ_c is quite low and fractal ϕ may exceed this value giving negatives K_m. Another approach to model the properties of unconsolidated sands is the CCT theory developed by Dvorkin et al. (1994) (see also Guo and Han 2016; Carcione et al. 2023).

Now, we obtain the porosity of the sand as a function of the pore pressure (the shale porosities are assumed to be constant). It is:

$$d\phi = -\left(\frac{1 - \phi}{K_m} - \frac{1}{K_s}\right) d(p_c - p). \tag{6}$$

(Carcione 2022). An approximation from Eq. (3) yields,

$$\phi = \phi_0 + \left(\frac{1 - \phi_0}{K_m} - \frac{1}{K_s}\right)(p - p_H), \tag{7}$$

where we have assumed $(1 - \phi)/K_m$ at p_H and a constant confining pressure at a given depth.

On the other hand, an implicit exact expression can be obtained from Eq. (5),

$$\frac{(1 - \phi_c)}{K_s}(p - p_H) = \phi_0 - \phi + \phi_c \ln \frac{\phi}{\phi_0}. \tag{8}$$

Table 1 Properties of the Sleipner model at 100 % brine saturation

Formation	ϕ_0 (%)	C (%)	ρ (kg/m^{-3})	v_P (km/s)	v_S (km/s)	κ_x (mD)	κ_z (mD)
Caprock	22	95	2218	2295	1010	0.97	0.097
Utsira	37	5	1991	2048	643	1926	193
Mudstone layers	24	85	2188	2283	973	1.66	0.16

In order to perform fluid-flow simulations (Carcione et al. 2014) and obtain the pore pressure and fluid saturation, the simulator needs the compressibility C_{pp}, according to the notation of Zimmerman et al. (1986), which is given by:

$$C_{pp} = \frac{1}{\phi}\left(\frac{1}{K_m} - \frac{1+\phi}{K_s}\right) \tag{9}$$

(Carcione 2022).

The fluid-flow simulations and modeling of seismic attenuation require the permeability. Carcione et al. (2000) derived a model of permeability as a function of clay content. They assume that a shaly sandstone is composed of a sandy matrix and a shaly matrix with partial permeabilities:

$$\kappa_q = \frac{R_q^2\phi^3}{45(1-\phi)^2(1-C)} \quad \text{and} \quad \kappa_c = \frac{R_c^2\phi^3}{45(1-\phi)^2 C}, \tag{10}$$

respectively, where R_q and R_c denote the average radii of sand and clay particles, respectively. Assuming that permeability is analogous to the inverse of the electrical resistance, we assume that the average permeability of the shaly sandstone along the horizontal direction is given by:

$$\frac{1}{\kappa_x} = \frac{1-C}{\kappa_q} + \frac{C}{\kappa_c} = \frac{45(1-\phi)^2}{R_q^2\phi^3}\left[(1-C)^2 + C^2\frac{R_q^2}{R_c^2}\right]. \tag{11}$$

In this work, we consider $R_q = 50$ μm and $R_c = 1.5$ μm, which gives $\kappa_x = 1.9$ Darcy (at ϕ_0) (Arts et al. 2008; Nilsen et al. 2011). It is the case that to obtain a realistic saturation map so that the post-injection synthetic seismogram resembles the real one, the permeability has to be defined to satisfy this requirement. In this case, the clay content is obtained from κ_x by solving the quadratic Eq. (11) in the variable C.

In anisotropic media, the permeability components depend on saturation in a different manner (Bear et al. 1987; Bear and Bachmat 1990; Carcione et al. 2003). This behavior can be modeled with the following horizontal and vertical dependence of permeability on saturation (Carcione et al. 2003): $[1-(1-0.3a)\sin(\pi S_w)]$ and $a[1-0.5\sin(\pi S_w)]$ where a is a permeability-anisotropy parameter. These equations model the rotation of the ellipses of directional permeability versus saturation obtained by Bear et al. (1987) by means of numerical experiments. Then, we have:

$$\frac{\kappa_x}{\kappa_z} = \frac{1-(1-0.3a)\sin\pi S_w}{a(1-0.5\sin\pi S_w)}. \tag{12}$$

Note that for $S_w = 0$ or 1, $\kappa_z = a\kappa_x$. A value of $a = 1/10$ is assumed here (Nilsen et al. 2011). It is $\kappa_x > \kappa_z$ at full water saturation, due to pore cross sections which are larger in the x-direction. As water saturation is reduced, and the larger pores drained first, a saturation is reached at which $\kappa_x = \kappa_z$. Then, as saturation is further reduced, $\kappa_x < \kappa_z$. At the other end (full gas saturation), we have again $\kappa_x > \kappa_z$.

The viscosity of the fluid is required for both the computation of synthetic seismograms including attenuation and the fluid-flow simulations. We assume that the viscosity of water is independent of pressure and temperature as an approximation, $\eta_w = 0.0018$ Pa s. For the gas viscosity η_g, we assume the equation proposed by Luo and Vasseur (1996). It depends on pore pressure and temperature T:

$$\eta_g[\text{Pa } s] = 10^{-5} + 1.5\times10^{-8}\frac{p}{\rho g} - 2.2\times10^{-7}(T - T_0), \tag{13}$$

where T_0 is the surface temperature.

The pre-injection P-wave velocity can be obtained from the Gassmann equation. The low-frequency bulk modulus of the wet rock is given by the Gassmann modulus:

$$K = K_m + \alpha^2 M, \tag{14}$$

where:

$$\alpha = 1 - \frac{K_m}{K_s} \quad \text{and} \quad M = \left(\frac{\alpha-\phi}{K_s} + \frac{\phi}{K_f}\right)^{-1}. \tag{15}$$

(e.g., Carcione 2022), where K_f is the fluid modulus.

When the fluids are not mixed in the pore volume, but distributed in patches, the effective bulk modulus of the fluid at high frequencies is higher than that predicted by Wood (Reuss) modulus. We then use White's mesoscopic model (Carcione et al. 2006) to obtain the P-wave velocity and quality factor (see below).

The pre-injection P-wave and S-wave velocities are then:

$$v_P = \sqrt{\frac{K + 4\mu_m/3}{\rho}} \quad \text{and} \quad v_S = \sqrt{\frac{\mu_m}{\rho}}. \tag{16}$$

The velocities of the Utsira Sand at p_H and full water saturation are $v_P = 2045$ m/s and $v_S = 641$ m/s in agreement with reported values (McKenna et al. 2003; Chadwick et al. 2005; Arts et al. 2008; Rabben and Ursin 2011).

The post-injection P-wave velocity and attenuation (quality factor) are obtained with the White model (see Fig. 7 in Carcione et al. 2006), which requires as input the fluid saturations, the size of the gas patches, the viscosities and the permeability of the sand. (The horizontal permeability is used.). The patch size has an important influence on attenuation.

In the pre-injection case (full brine saturation), this model predicts no wave-energy loss (Carcione et al. 2006). Shear waves are assumed to be lossless. We also consider the possibility that CO_2 can go into solution in the brine. This process affects the saturation of the gaseous phases and the density and bulk moduli of the liquid phases (see Carcione et al. 2006). We model the thin mudstone layers with $C = 85$ % and $\phi_0 = 24$ %, while the caprock values are $\phi_0 = 22$ % and $C = 95$ %.

We consider that the layer underlying the Utsira formation has the same properties of the caprock. Table 1 summarizes the properties of the different formations at 100 % saturation. The initial porosity and clay content models are shown in Fig. 1. The thin mudstone layers can be seen as black lines in the Utsira formation. We have used fluid-flow simulations, based on the theory in Carcione et al. (2014), to build the post-injection model.

Synthetic seismograms

We first consider the pre-injection case at full water saturation. Figure 2 shows the *P*- and *S*-wave velocity panels (a, b) and the density panel c. The synthetic seismograms are

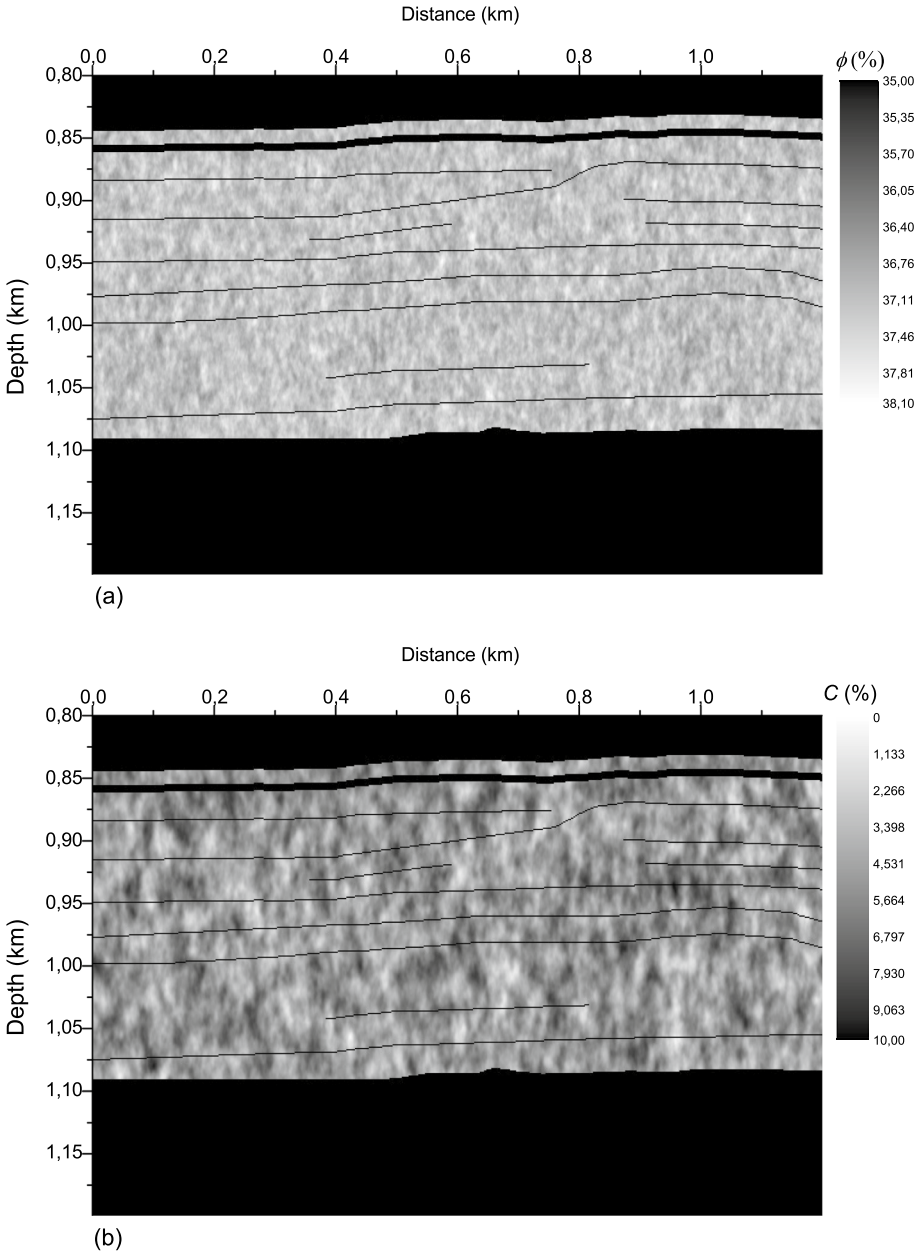

Fig. 1 Porosity ϕ_0 **a** and clay content C **b** panels. The bars indicate the variations in the Utsira sandstone. The thin mudstone layers have $C = 85$ % and $\phi_0 = 24$ % and the caprock and lower medium have $\phi_0 = 22$ % and $C = 95$ %

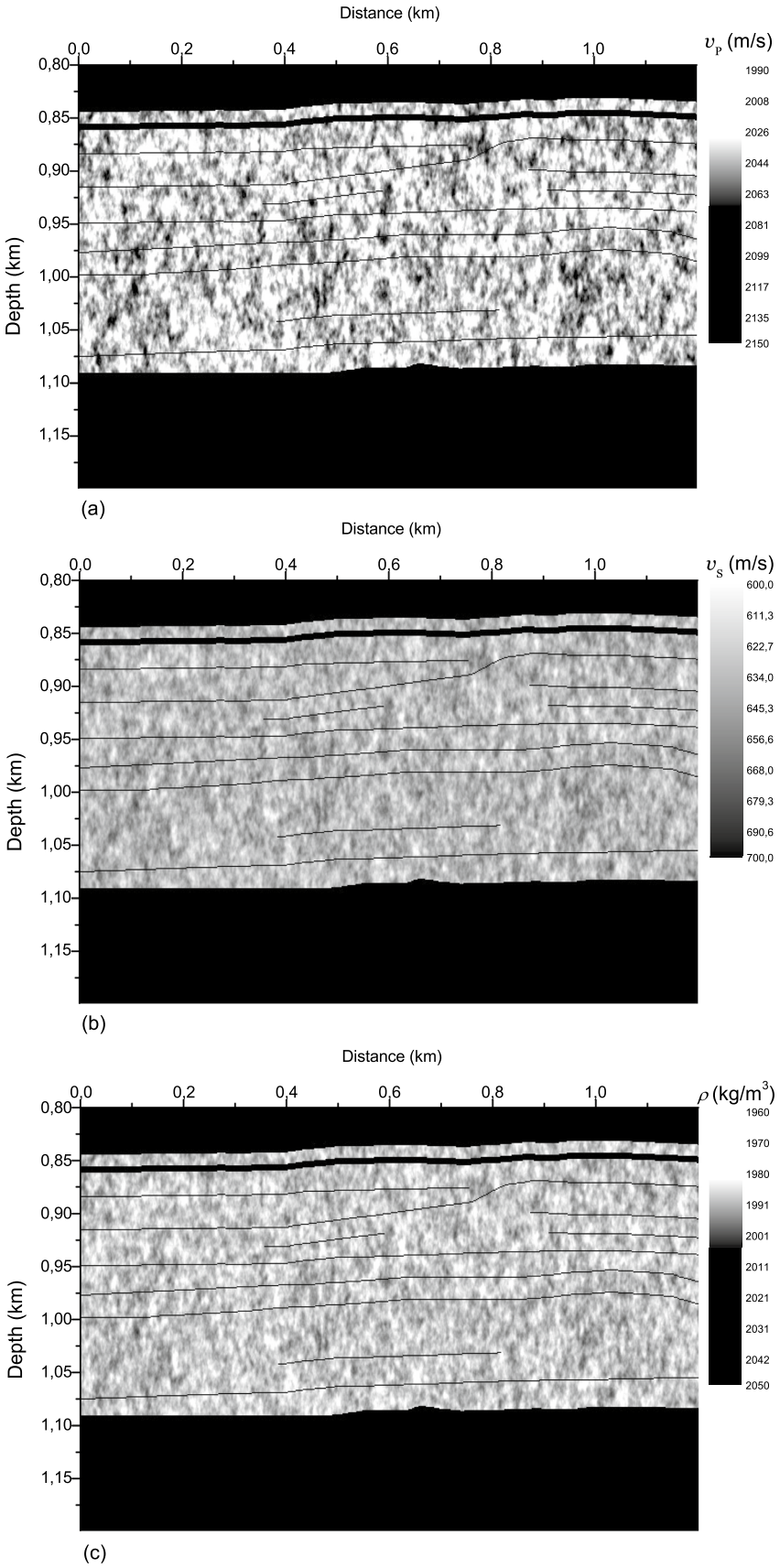

Fig. 2 *P*- and *S*-wave velocity (**a**, **b**) and density **c** models corresponding to pre-injection. The bar ranges indicate the variations in the Utsira formation. The values for the caprock and mudstone layers are given in Table 1

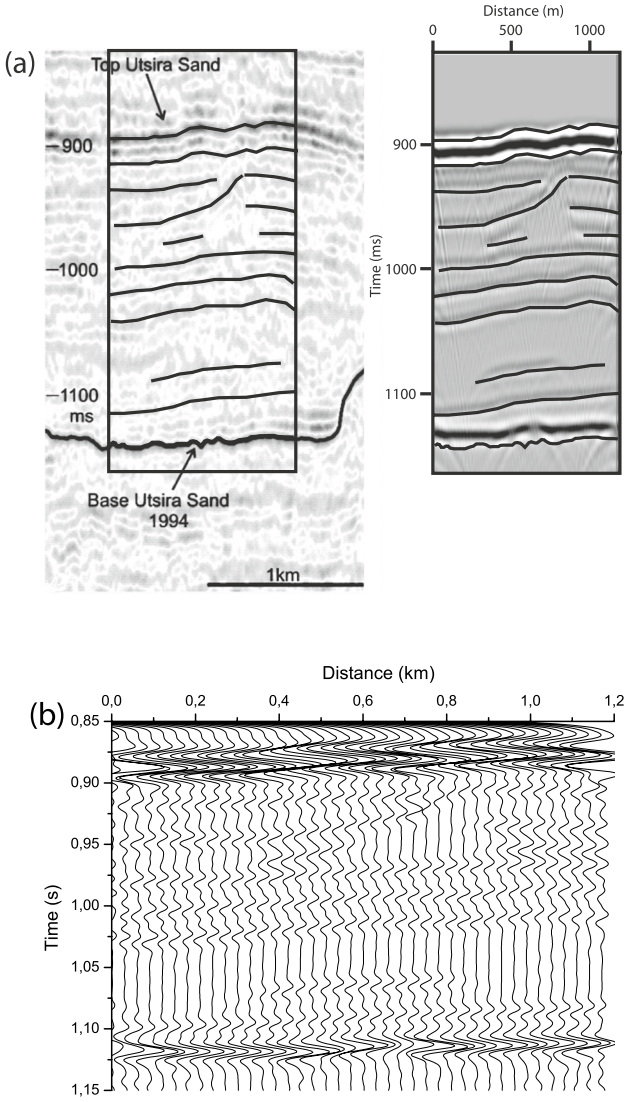

Fig. 3 Comparison between the real (left) and synthetic (right) seismograms **a** and wiggle-trace version of the synthetic seismogram **b** before the injection (real data from Chadwick et al., 2004)

computed with a modeling code based on an isotropic and viscoelastic stress–strain relation. The equations are given in Section "Synthetic seismograms" of Carcione (2022) and in Carcione et al. (2012). The algorithm is based on the Fourier pseudospectral method for computing the spatial derivatives and a fourth-order Runge–Kutta technique for calculating the wavefield recursively in time. As stated above, the *P*-wave velocity and quality factor are those predicted by White's model, where we consider the central frequency of the source f_0. The modeling approximates the relaxation peak with a Zener element whose peak frequency is f_0 and White's velocity at this frequency. Details can be found in Carcione et al. (2012).

The grid has 1200×400 points, with squared cells of 1 m size, and the source is a Ricker-type wavelet with a central frequency $f_0 = 50$ Hz. A localized plane wave acts as a source above the top of the aquifer. Figure 3 compares the real (left) and synthetic (right) seismograms a and wiggle-trace version of the synthetic seismogram b before the injection. Simulations and real data show a remarkable match.

Carbon dioxide has been injected at Sleipner a constant flow rate of one million tons per year. The fluid-flow simulator computes the post-injection model of saturation and pore pressure. There are preferential pathways or openings through the mudstone thin layer, where the CO_2 migrates upwards. In those locations the permeability of the medium is assumed to be 0.6 D. The CO_2 saturation and pore pressure after two years of injection are shown in Fig. 4a and b, respectively. The CO_2 has accumulated below the intra-reservoir mudstones as reported by Chadwick et al. (2005).

Knowledge of pore pressure allows us to obtain the bulk modulus and density of the gas phase as a function of depth by using the Peng–Robinson equation of state (Picotti et al. 2012). The size of the gas patches in White's model is 0.05 m (see Carcione et al. (2012) for more details). Figure 5 shows the post-injection *P*-wave velocity a, density b and *Q*-factor c panels. The latter are those at the central frequency of the source f_0. The *P*-wave velocity has substantially decreased in the aquifer compared to the full water saturation case. The low *Q*-factors indicate the high wave-energy attenuation within the aquifer due to wave-induced fluid flow.

Finally, Fig. 6 compares the pre-injection (a) and post-injection (b) seismograms. Panel c corresponds to the difference between the post-injection elastic and viscoelastic simulations. The deeper events show higher amplitudes, as expected, due to the stronger effect of the finite *Q* factor of the layers. This underlines the importance of considering attenuation in computing reliable synthetic data. A statistical analysis of the detectability of the time-lapse signal can be done with the method proposed by Alajmi et al. (2016).

Conclusions

We propose a monitoring methodology based on a petrophysical model, fluid-flow and wave simulations for a seismic characterization of formations partially saturated with carbon dioxide. The methodology has been applied

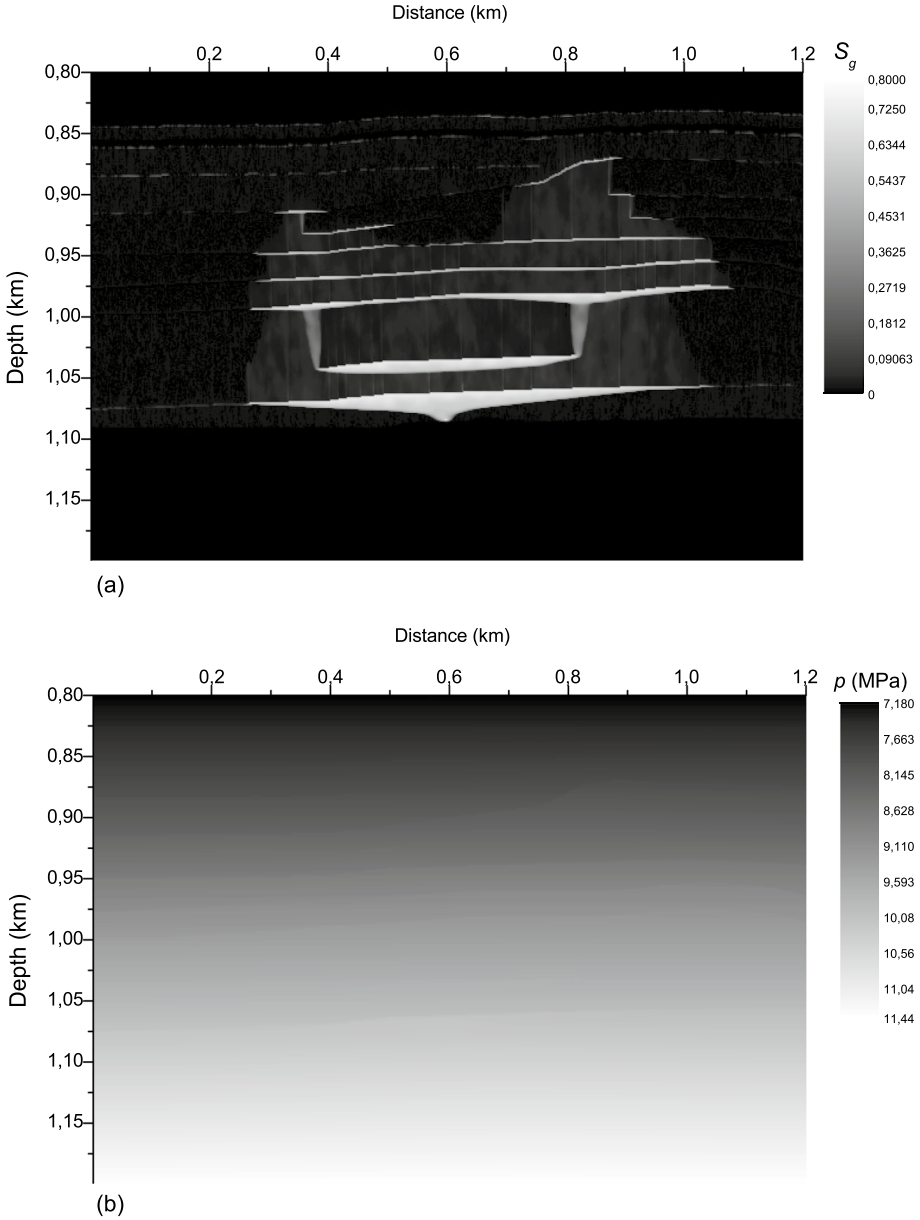

Fig. 4 CO_2 saturation **a** and pore pressure **b** panels after two years of injection

to the Sleipner field in the North Sea, but can be used for another storage site, provided that the in situ pressure and temperature conditions can be computed and well logs are available to calibrate the model. The workflow consists of (1) building a preliminary geological model on the basis of porosity and clay content or permeability; (2) performing fluid-flow simulations to obtain a map of partial saturation and pore pressure; (3) calculating the wave velocities, density and attenuation factor at different injection stages; (4) generating synthetic seismograms and comparing these to the real data to refine the model. The methodology can first be used to test the performance of seismic inversion algorithms to detect the presence of gas and quantify its partial saturation. Use of a mesoscopic-loss model based on White's theory describes the *P*-wave quality factor, which can be inverted with attenuation tomography and obtain more information on the formation properties such as porosity and permeability. The technique can be applied to CO_2 storage problems or the detection of gas in hydrocarbon reservoirs.

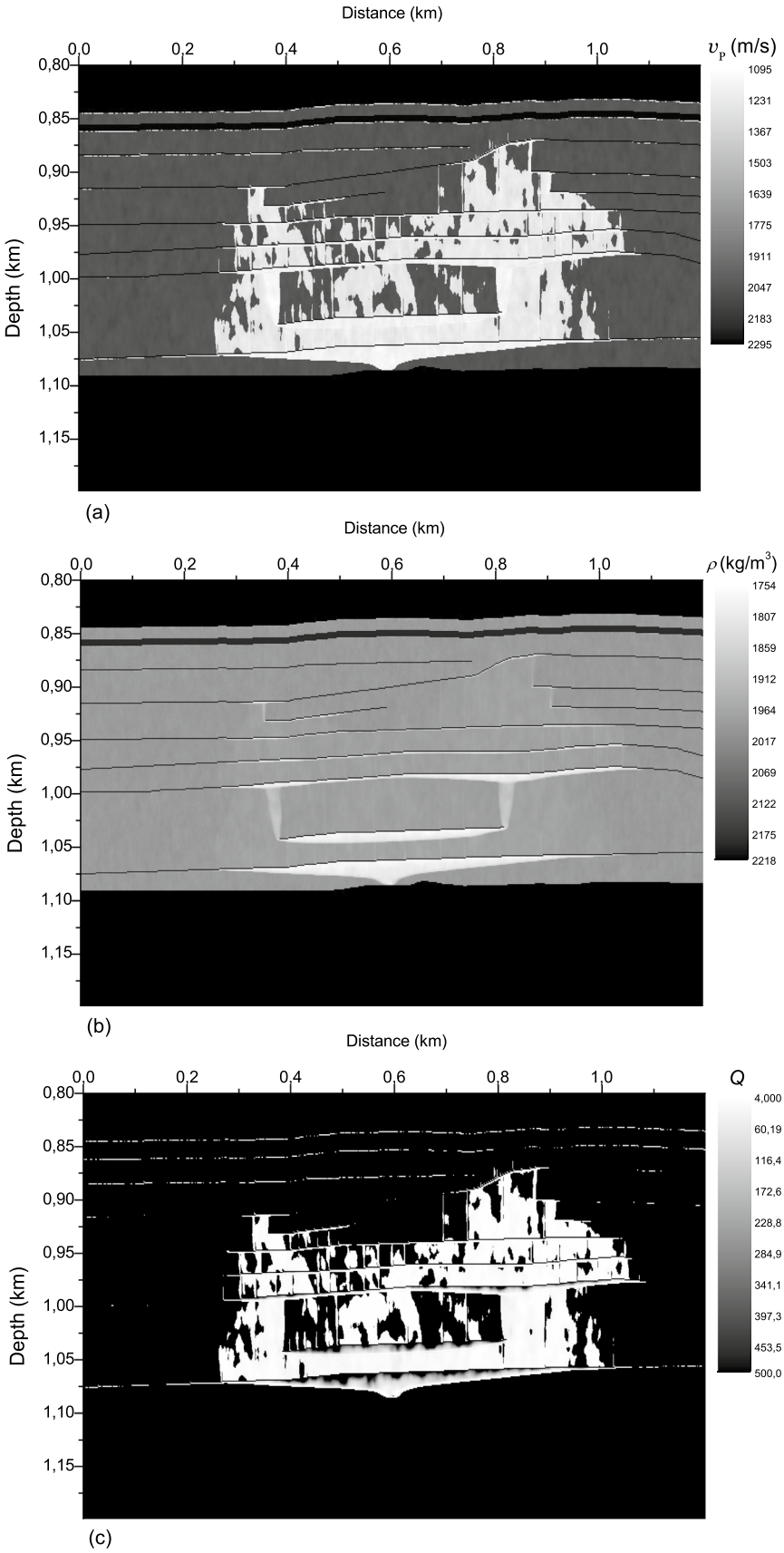

Fig. 5 Post-injection *P*-wave velocity **a**, density **b** and *Q*-factor **c** panels

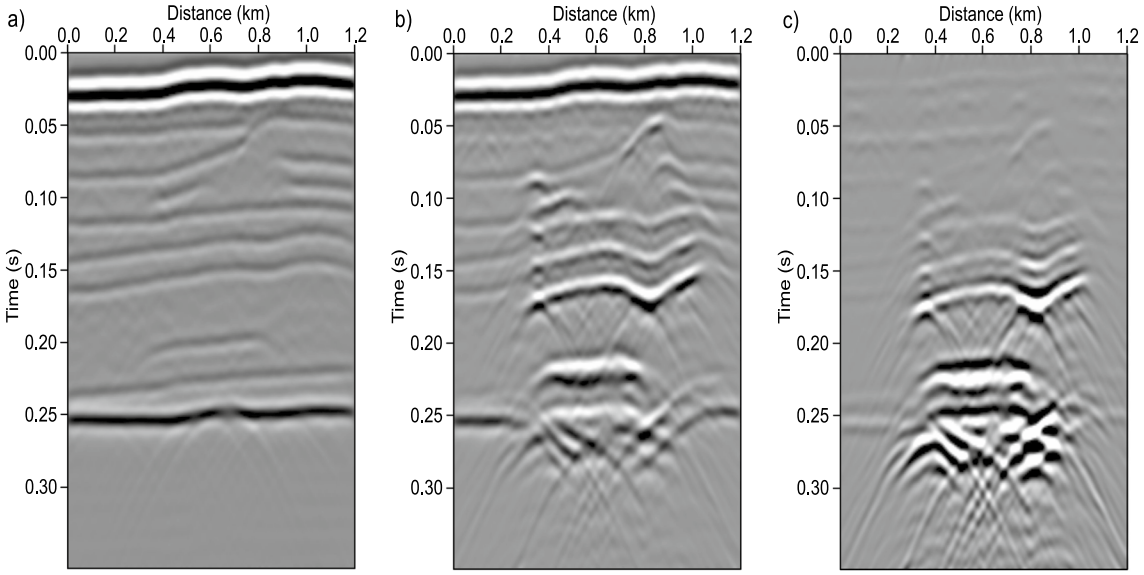

Fig. 6 Comparison between the pre-injection **a** and post-injection **b** synthetic seismograms and difference between the elastic (lossless) and viscoelastic (lossy) cases **c**. The latter shows events due to the effect of finite Q-factors

Acknowledgements We thank Prof. Junxin Guo for useful comments.

Author contributions MA edited the manuscript and coded the programs. DG made and discussed the plots. JMC re-coded the programs and provided the concept. ANQ conducted the literature review. JS and JB reproduced the plots and wrote some sections.

Funding This work is supported by the National Natural Science Foundation of China (grant no. 41974123 and 42174161), and National Natural Science Foundation of China (NSFC) National Science Fund for Distinguished Young Scholars (BK20200021).

Declarations

Conflict of interest The authors declare that they have no conflict of interest.

Consent to publish The Authors confirm that the work described has not been published before and is not under consideration for publication elsewhere. Its publication has been approved by all co-authors and the responsible authorities at the institutions where the work is carried out.

References

Alajmi M, Bona A, Pevzner R (2016) Empirical 3D depth/time dependent coherent noise generation for use in statistical models of seismic data. J Appl Geophys 125:7–13

Arts RJ, Chadwick A, Eiken O, Thibeau S, Nooner S (2008) Ten years' experience of monitoring CO_2 injection in the Utsira Sand at Sleipner, offshore Norway. First Break 26:65–72

Arts R, Eiken O, Chadwick A, Zweigel P, van der Meer L, Zinszner B (2004) Monitoring of CO2 injected at Sleipner using time-lapse seismic data. Energy 29:1383–1392

Audigane P, Gaus I, Czernichowski-Lauriol I, Pruess K, Xu T (2007) Two-dimensional reactive transport modeling of CO2 injection in a saline aquifer at the Sleipner site. North Sea Am J Sci 307:974–1008

Audigane P, Chiaberge C, Mathurin F, Lions J, Picot-Colbeaux G (2011) A workflow for handling heterogeneous 3D models with the TOUGH2 family of codes: applications to numerical modeling of CO2 geological storage. Comput Geosci 37:610–620

Bear J, Bachmat Y (1990) Introduction to modeling of transport phenomena in porous media. Kluwer, Dordrecht

Bear J, Braester C, Menier PC (1987) Effective and relative permeabilities of anisotropic porous media. Transp Porous Med 2:301–316

Carcione JM (2022) Wave fields in real media. Theory and numerical simulation of wave propagation in anisotropic, anelastic, porous and electromagnetic media, 4th edition, Elsevier

Carcione JM, Gei D (2009) Theory and numerical simulation of fluid-pressure diffusion in anisotropic porous media. Geophysics 74:N31–N39

Carcione JM, Gei D, Picotti S, Michelini A (2012) Cross-hole electromagnetic and seismic modeling for CO2 detection and monitoring in a saline aquifer. J Petrol Sci Eng. https://doi.org/10.1016/j.petrol.2012.03.018

Carcione JM, Gurevich B, Cavallini F (2000) A generalized Biot–Gassmann model for the acoustic properties of shaley sandstones. Geophys Prosp 48:539–557

Carcione JM, Helbig K, Helle HB (2003) Effects of pressure and saturating fluid on wave velocity and attenuation of anisotropic rocks. Int J Rock Mech Min Sci 40:389–403

Carcione JM, Picotti S, Gei D, Rossi G (2006) Physics and seismic modeling for monitoring CO2 storage. Pure Appl Geophys 163:175–207

Carcione JM, Picotti S, Santos JE, Qadrouh AN, Almalki HS (2014) Numerical simulation of two-phase fluid flow. J Petrol Explor Prod Technol. https://doi.org/10.1007/s13202-014-0109-y

Carcione JM, Qadrouh AN, Alajmi M, Alqahtani NB, Ba J (2023) Rock acoustics of CO2 storage in basalt. Geophys J Int. https://doi.org/10.1093/gji/ggad252

Chadwick RA, Arts R, Eiken O (2005) 4D seismic quantification of a growing CO_2 plume at Sleipner North Sea. In: Dore, A.G.; Vining, B.A., (eds.) Petroleum geology: North-West Europe and

global perspectives—proceedings of the 6th petroleum geology conference. Geological Society, London, pp 1385-1399
Chadwick A, Noy D, Lindeberg E, Arts R, Eiken O, Williams G (2006) Calibrating reservoir performance with time-lapse seismic monitoring and flow simulations of the Sleipner CO2 plume. GHGT-8: 8th International conference on greenhouse gas control technologies, Trondheim, Norway, 19–22 June 2006. Elsevier, Oxford, pp 1–6
Dupuy B, Romdhane A, Eliasson P, Querendez E, Yan H, Torres VA, Ghaderi A (2017) Quantitative seismic characterization of CO2 at the Sleipner storage site. North Sea Interpret 5(4):23–42. https://doi.org/10.1190/INT-2017-0013.1
Dvorkin J, Nur A, Yin H (1994) Effective properties of cemented granular material. Mech Mater 18:351–366
Ganguli SS, Kumar P, Dimri VP (2019) Seismic anisotropy of a fractured rock during CO2 injection: a feasibility study. Acta Geophys 67:141–148
Guo J, Han X (2016) Rock physics modelling of acoustic velocities for heavy oil sand. J Petrol Sci Eng 145:436–443
Liao J, Wen P, Guo J, Zhou L (2023) Seismic dispersion, attenuation and frequency-dependent anisotropy in a fluid-saturated porous periodically layered medium. Geophys J Internat 234:331–345
Luo X, Vasseur G (1996) Geopressuring mechanism of organic matter cracking: numerical modeling. AAPG Bull 80:856–874
Mavko G, Mukerji T, Dvorkin J (2009) The Rock physics handbook. Cambridge University Press
McKenna JJ, Gurevich B, Urosevic M, Evans BJ (2003) Rock physics-application to geological storage of CO_2. APPEA Journal 43:567–576
Nilsen HM, Herrera PA, Ashraf SM, Ligaarden I, Iding M, Hermanrud C, Lie K-A, Nordbottem JM, Dahle HK, Kellegavlen E (2011) Field-case simulation of CO_2-plume migration using vertical-equilibrium models. Energy Proced 4:3801–3808
Picotti S, Carcione JM, Gei D, Rossi G, Santos JE (2012) Seismic modeling to monitor CO_2 geological storage: the Atzbach-Schwanenstadt gas field. J Geophys Res 117:B06103. https://doi.org/10.1029/2011JB008540
Rabben TE, Ursin B (2011) AVA inversion of the top Utsira Sand reflection at the Sleipner field. Geophysics 76:C53–C63
Savioli G, Santos JE (2011) Modeling of CO_2 storage in aquifers. J Phys Conf Ser 296:012021. https://doi.org/10.1088/1742-6596/296/1/012021
Savioli GB, Santos JE, Carcione JM, Gei D (2016) A model for CO2 storage and seismic monitoring combining multiphase fluid flow and wave propagation simulators. Sleipner-field Case Comput Geosci. https://doi.org/10.1007/s10596-016-9607-y
White MD, Oostrom M, Imhard RJ (1995) Modeling fluid flow and transport in variably saturated porous media with the STOMP simulator. 1. Nonvolatile three-phase model description. Adv Water Res 18(6):353–364
Zimmerman RW, Somerton WH, King MS (1986) Compressibility of porous rocks. J Geophys Res 91:12765–12777